tvst

DOI: 10.1167/tvst.4.4.3

Article

Characterizing the Impact of Off-Axis Scan Acquisition on the Reproducibility of Total Retinal Thickness Measurements in SDOCT Volumes

Bhavna J. Antony[1,2], Paul F. Stetson[3], Michael D. Abramoff[4,5], Kyungmoo Lee[5], Johanna M. Colijn[6,7], Gabriëlle H. S. Buitendijk[6,7], Caroline C. W. Klaver[6,7], Austin Roorda[1,2], and Brandon J. Lujan[1,8]

[1] School of Optometry, University of California Berkeley, CA, USA
[2] Vision Science Graduate Group, University of California Berkeley, CA, USA
[3] Carl Zeiss Meditec, Inc., Dublin, CA, USA
[4] Wynn Institute for Vision Research, University of Iowa, Iowa City, IA, USA
[5] Electrical and Computer Engineering, University of Iowa, Iowa City, IA, USA
[6] Department of Ophthalmology, Erasmus Medical Center, Rotterdam, the Netherlands
[7] Department of Epidemiology, Erasmus Medical Center, Rotterdam, the Netherlands
[8] West Coast Retina Medical Group, San Francisco, CA, USA

Correspondence: Brandon Lujan, School of Optometry, University of California Berkeley, CA, USA; blujan@berkeley.edu 0

Received: 5 December 2014
Accepted: 31 May 2015
Published: 31 July 2015

Keywords: total retinal thickness; off-axis scans; Stiles-Crawford effect; SDOCT

Citation: Antony BJ, Stetson PF, Abramoff MD, et al. Characterizing the impact of off-axis scan acquisition on the reproducibility of total retinal thickness measurements in SDOCT volumes. Trans Vis Sci Tech. 2015;4(4):3, doi:10.1167/tvst.4.4.3

Purpose: Off-axis acquisition of spectral domain optical coherence tomography (SDOCT) images has been shown to increase total retinal thickness (TRT) measurements. We analyzed the reproducibility of TRT measurements obtained using either the retinal pigment epithelium (RPE) or Bruch's membrane as reference surfaces in off-axis scans intentionally acquired through multiple pupil positions.

Methods: Five volumetric SDOCT scans of the macula were obtained from one eye of 25 normal subjects. One scan was acquired through a central pupil position, while subsequent scans were acquired through four peripheral pupil positions. The internal limiting membrane, the RPE, and Bruch's membrane were segmented using automated approaches. These volumes were registered to each other and the TRT was evaluated in 9 Early Treatment of Diabetic Retinopathy Study (ETDRS) regions. The reproducibility of the TRT obtained using the RPE was computed using the mean difference, coefficient of variation (CV), and the intraclass correlation coefficient (ICC), and compared to those obtained using Bruch's membrane as the reference surface. A secondary set of 1545 SDOCT scans was also analyzed in order to gauge the incidence of off-axis scans in a typical acquisition environment.

Results: The photoreceptor tips were dimmer in off-axis images, which affected the RPE segmentation. The overall mean TRT difference and CV obtained using the RPE were 7.04 $\pm$ 4.31 μm and 1.46%, respectively, whereas Bruch's membrane was 1.16 $\pm$ 1.00 μm and 0.32%, respectively. The ICCs at the subfoveal TRT were 0.982 and 0.999, respectively. Forty-one percent of the scans in the secondary set showed large tilts ($>$ 6%).

Conclusions: RPE segmentation is confounded by its proximity to the interdigitation zone, a structure strongly affected by the optical Stiles-Crawford effect. Bruch's membrane, however, is unaffected leading to a more robust segmentation that is less dependent upon pupil position.

Translational Relevance: The way in which OCT images are acquired can independently affect the accuracy of automated retinal thickness measurements. Assessment of scan angle in a clinical dataset demonstrates that off-axis scans are common, which emphasizes the need for caution when relying on automated thickness parameters when this component of scan acquisition is not controlled for.

translational vision science & technology

Introduction

Optical coherence tomography (OCT) is used frequently for the diagnosis and management of a variety of retinal diseases.[1–4] The introduction of spectral domain OCT systems (SDOCT) provided an improvement in image quality compared to time domain systems,[5,6] and also dramatically improved speed, allowing for volumetric imaging.[4,7] The development of numerous retinal layer segmentation approaches further allowed for the automated assessment of retinal parameters, such as the total retinal thickness (TRT), and for the tracking of disease progression over time.

Off-axis acquisition of SDOCT scans has been shown to affect TRT estimates (Antony et al. *IOVS* 2014;55:ARVO E-Abstract 4791), where increases up to 33 μm have been reported.[8] In these scans, measuring retinal layers axially along A-scans[9] will induce an artifactual thickness increase due to the geometry of the structure. However, the observed increases in TRT are larger than what will arise from this simple geometrical effect, which we show later in this report to be only 1.91% for an angle of 11.13°. Thus, the angle-dependent thickness increase cannot be attributed to the geometry alone.

Segmentation accuracy in SDOCT volumes could be affected by a variety of factors, such as the presence of retinal pathology,[10] density of B-scans obtained in a volume,[11] and axial length of the eye.[12] While these have been recognized as sources of error, none of these factors can completely explain the systematic thickness changes due to alteration in the pupil entry position.

The optical correlate of the Stiles-Crawford effect[13] has been described as the change in photoreceptor light acceptance and reflectivity as a function of angle relative to its axis, or pointing direction.[14,15] It has been shown to affect the reflectivity of the inner segment-outer segment junction (IS/OS) and the posterior tips of the outer segments (PTOS).[16–18] These structures appear dimmer in scans acquired through noncentral (or off-axis) pupil locations than in on-axis scans. The appearance of structures in SDOCT images is crucial as automated segmentation approaches typically use sharp changes in intensity, referred to as gradients, to identify retinal layer boundaries. The distinct gradient at the PTOS is particularly relevant as many automated segmentation approaches segment the PTOS in lieu of the lower boundary of the retinal pigment epithelium (RPE).[19–24]

The TRT usually is defined using the location of the internal limiting membrane (ILM) as the upper boundary and either the RPE or Bruch's membrane as the lower reference surface. Thus, variability in the RPE segmentation could strongly impact the TRT estimate.

To characterize and quantify the impact of off-axis scan acquisition on TRT estimates, we compared the reproducibility when using either the RPE or Bruch's membrane as the lower reference surface. Additionally, the error that would be induced by the geometry in the off-axis scans also was computed to provide an estimate of the expected changes in TRT.

Methods

Data

The Western Institutional Review Board approved the protocol, each subject gave written informed consent to participate in the study, and the Declaration of Helsinki guidelines were followed throughout the study. Patients were dilated using 2.5% phenylephrine and 1% tropicamide. Subjects were screened for a normal macula without retinal pathology.

Volumetric SDOCT images were acquired from 25 normal subjects on Cirrus HDOCT (Carl Zeiss Meditec, Inc., Dublin, CA). The images were obtained from a $6 \times 6 \times 2$ mm region centered on the fovea containing $512 \times 128 \times 1024$ voxels. For the first scan, the pupil entry location was chosen carefully so that the B-scans in the horizontal and vertical directions appeared "flat" (see Fig. 1A). Subsequently, four more scans were obtained so that the scan appeared "tilted" in the horizontal and vertical directions as depicted in Figure 1B.[25]

Retinal Thickness

The TRT was defined in two ways, using the ILM as the upper reference surface and either the RPE or Bruch's membrane as the lower reference surface. Total retinal thickness based on the distance between the ILM and RPE was segmented using a Carl Zeiss (Carl Zeiss Meditec, Inc.) prototype version of the Cirrus algorithm. Total retinal thickness based on the distance between the ILM and Bruch's membrane (visualized as the bottom of the RPE/Bruch's membrane complex in SDOCT images) was segmented using the Iowa Reference Algorithm.[19,26,27]

Before assessing the thickness, the volume scans acquired from different pupil positions the off-axis scans were registered to the on-axis scan.[28] The retinal vasculature was visualized in projection images, which were created by averaging the A-scans between the IS/

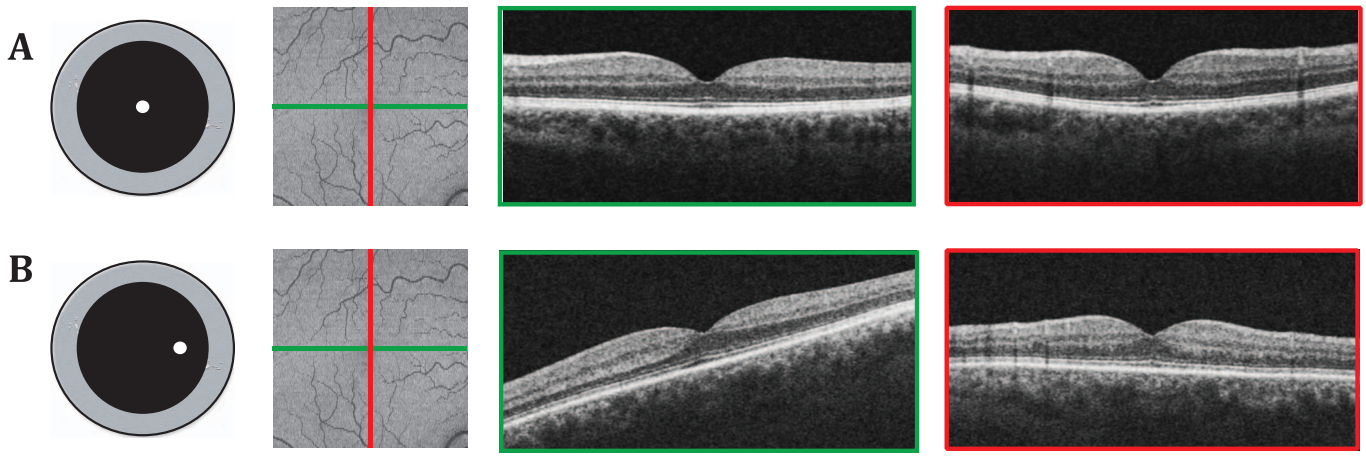

Figure 1. Illustration depicting on-axis and off-axis scans. The on-axis scan (*top row*) is acquired by selecting a pupil location so that the B-scans in the horizontal (marked in *green*) and the vertical (marked in *red*) directions appear flat. The off-axis scan is acquired by selecting a pupil location eccentric to the previous location. Here, a location to the right of the on-axis scan pupil position induces a tilt in the B-scan (marked in *green*) corresponding to the horizontal direction. Similarly, a pupil location above or below the on-axis scan pupil location would induce a tilt in the B-scan corresponding to the vertical axis.

OS junction and Bruch's membrane. A MATLAB (MathWorks, Natick, MA) user interface was used to manually select the correspondence points in the projection images (usually vessel branching points), which then were used to estimate the transformation (rotation and translation) parameters.[29] The TRT maps created using the on- and off-axis scans from a single subject then were transformed using the estimated transformation matrix, bringing all the TRT maps of the subject into the same reference frame. The average total retinal thickness in micrometers was computed in nine regions (Fig. 2), where the three concentric circles centered on the fovea have diameters of 1, 3, and 5 mm, respectively, and the sectors are 90° wide.

Angular Deviation

In addition to assessing the TRT, the angle of "tilt" in the images also was estimated. First, a plane was fit to the subfoveal region of the segmented Bruch's membrane. The normal to this then was used to estimate the angular deviation with respect to the *z*-axis (vertical depth axis) as depicted in Figure 3. The anisotropy of the voxel scale was corrected before the angle was computed.

The geometrical errors due to oblique scan angles were corrected as $T = T'*\cos\theta$, where T' is the measured thickness and T is the correct thickness. This simple correction assumes that no refraction takes place at any of the retinal interfaces between the ILM and posterior retina. If, for example, the retina

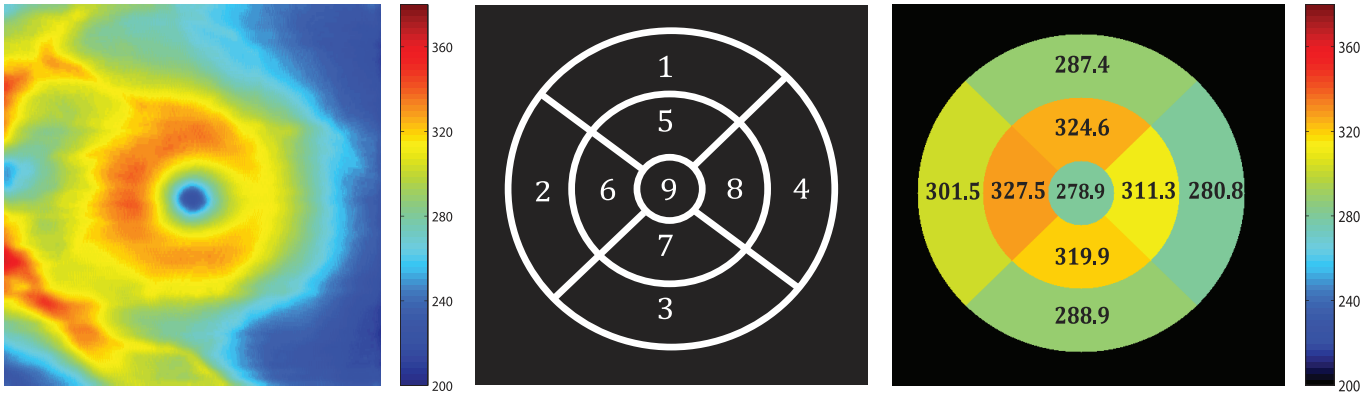

Figure 2. (A) The total retinal thickness is computed using the segmented ILM and Bruch's membrane. The average thickness is then computed within (B) the nine sectors defined by 3 concentric circles 1, 3, and 5 mm in diameter, respectively. (C) The average thickness in the nine sectors.

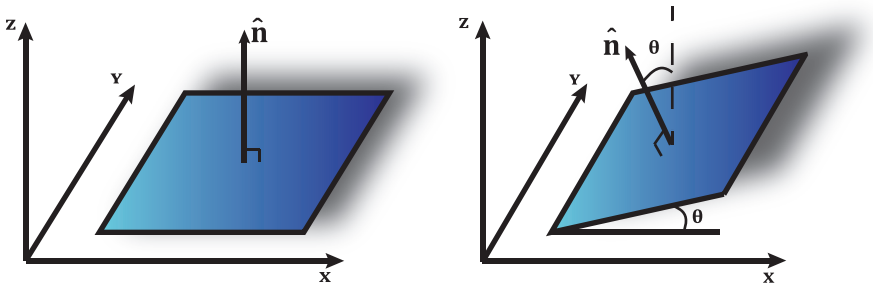

Figure 3. Illustration of the plane fit to the subfoveal region of the segmented Bruch's membrane. The angle θ was computed with respect to the vertical *z*-axis.

had an overall higher refractive index than the vitreous, an obliquely incident OCT beam would be refracted toward the normal to the retina surface, thereby diminishing the angle-dependent thickness artifacts. However, these secondary effects are expected to be negligible. This expected trigonometric change was computed for the scans and compared to the changes in thickness observed when using the RPE or Bruch's membrane.

Assessing Reproducibility of Thickness Measures

The TRT measurements in the nine Early Treatment of Diabetic Retinopathy Study (ETDRS) regions in the on-axis scans were compared to those obtained in the off-axis scans by computing the mean unsigned difference (mean ± SD μm). As multiple off-axis scans were available, the mean unsigned difference was averaged across these scans. The mean difference obtained when using the RPE as the reference surface was statistically compared to the mean difference obtained with Bruch's membrane using a paired *t*-test.

In addition, the coefficient of variation (CV%), expressed as the ratio of the standard deviation of the difference of the thickness measurements to the mean thickness measurement observed in the flat scans, as well as the intraclass correlation coefficient (ICC) and its corresponding 95% confidence interval were computed. These statistical tests were performed using the statistical package R.[30,31]

Table 1. Summary of the Reproducibility of the TRT When Using the RPE and Bruch's Membrane as the Reference Surface

Statistic	RPE	Bruch's Membrane
Mean ± SD, μm	7.04 ± 4.31	1.16 ± 1.00
CV, %	1.50	0.29
ICC[a]	0.982	0.999
95% CI[a]	(0.958, 0.992)	(0.997, 0.999)

[a] The central TRT ICC; the ICC for the remaining sectors are shown in Figure 5.

Incidence Rates of Off-Axis Scans

To gauge the prevalence of off-axis scan acquisition in a typical data acquisition environment, a second set of scans also were analyzed retrospectively. This dataset consisted of 2172 macular SDOCT scans obtained from one eye of 2172 subjects participating in the Rotterdam Study, a prospective population-based cohort study investigating age-related disorders.[32–34] This study population consisted of 14,925 individuals aged 45 years or older living in the Ommoord district of Rotterdam, The Netherlands. These scans were acquired on a SDOCT 1000 spectral-domain scanner (Topcon Corp., Tokyo, Japan) and imaged an area 6 × 6 × 2 mm and had dimensions of 512 × 128 × 665 voxels or 512 × 128 × 896 voxels.

Scans that showed acquisition-associated errors, such as clipped corners, were excluded. Scans acquired from myopic subjects also were excluded, as the retinal curvature in these scans is typically larger than in emmetropes. The angular deviation was computed for the final set of 1545 good quality scans using the steps described above.

Results

The results of the reproducibility analysis have been summarized in Table 1, which indicates that the reproducibility of TRT when using Bruch's membrane as the reference surface is better than when using the RPE. Figure 4 shows the mean difference, CVs, and ICCs within the nine regions. The overall

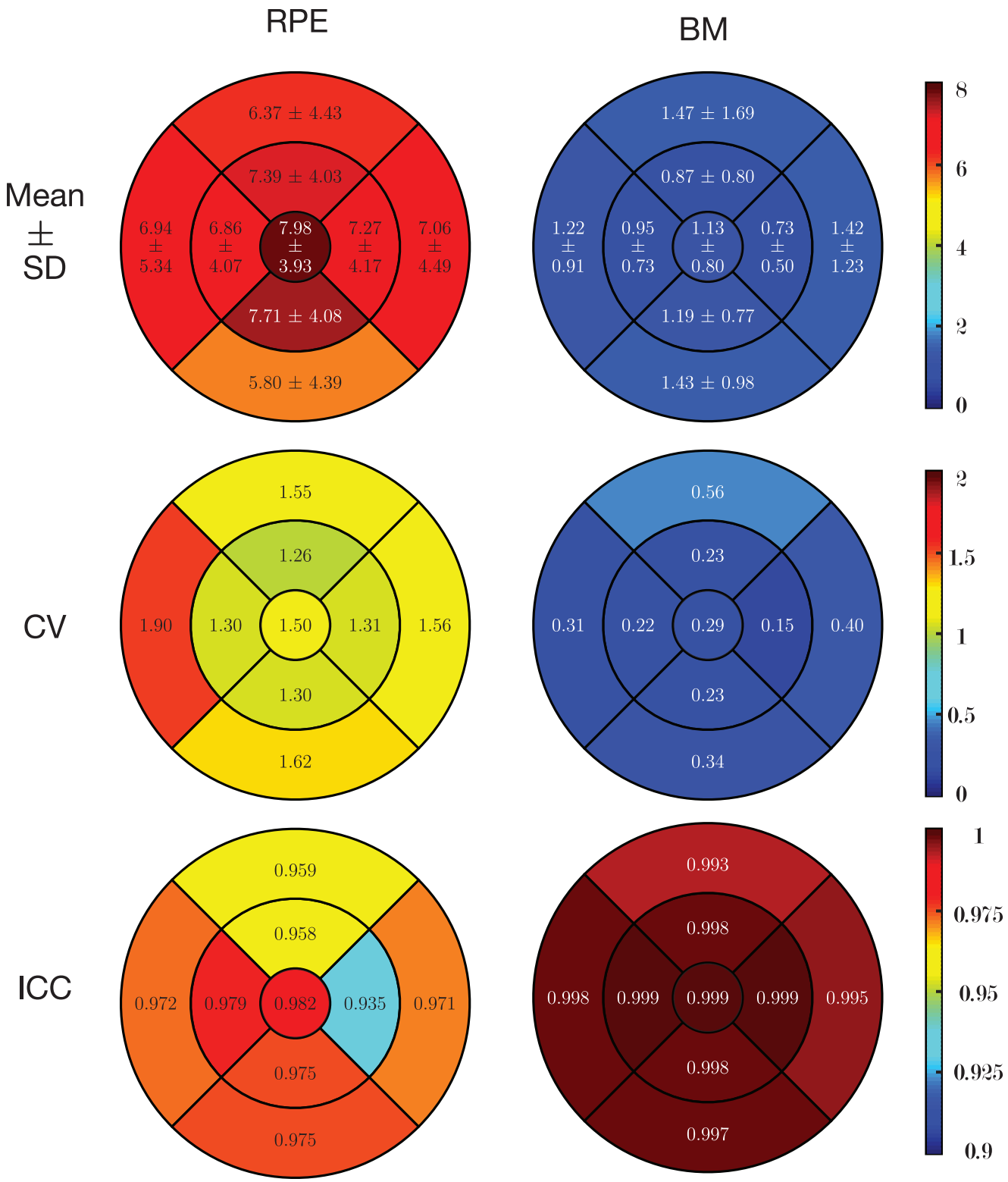

Figure 4. An illustration of the reproducibility of the TRT when using the RPE and Bruch's membrane as the reference surfaces. The *top row* shows the mean ± SD (μm), the *middle row* shows the CV%, and the *bottom row* shows the ICC.

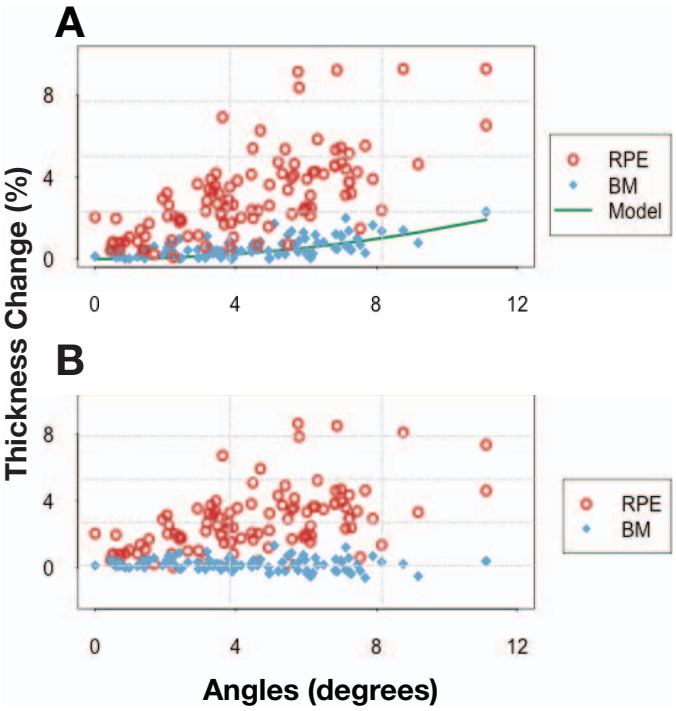

Figure 5. (A) Scatterplot depicting the change in TRT (%) when using the RPE (*red circle*) and Bruch's membrane (*blue diamond*) as the reference surface with respect to the angle of tilt in the images. The geometry-induced error that was modeled (*green*) is presented for comparison. (B) The thickness change (%) noted when using the RPE and Bruch's membrane after accounting for the geometry-induced errors.

mean difference in TRT when using the RPE was 7.04 ± 4.31 μm (2.39%) and when using Bruch's membrane as the reference surface was 1.16 ± 1.00 μm (0.32%). The mean difference in each of the nine regions also was statistically compared using a paired *t*-test, where the estimates using Bruch's membrane were significantly smaller ($P < 0.001$) than the mean difference obtained when using the RPE. The overall CVs (%) in the TRT measurements when using the RPE and Bruch's membrane as the reference surface were 1.46% and 0.30%, respectively. The ICC and its corresponding 95% confidence interval for the central TRT were 0.982 (0.958, 0.992) and 0.999 (0.997, 0.999), respectively.

Figure 5A shows a scatterplot of the change in TRT (%) with respect to the angular deviation computed from the images. The use of the RPE as the reference surface not only induced a significantly larger error than when Bruch's membrane is used, but the variability was also larger. The geometric error associated with measuring the TRT axially along each A-scan also was modeled and is indicated in the scatterplot in green. The largest angle noted in the dataset was 11.13° and the error induced by the geometry was 1.91%. However, the errors noted for the same scan when using the RPE as the reference surface was 6.52%, whereas with Bruch's membrane it was 2.30%. The larger standard deviation noted in the mean difference when using the RPE as the reference surface also is evident in the scatterplot. Figure 5B shows a scatterplot of the change in TRT (%) after accounting for the geometry-induced error. The change in TRT noted for Bruch's membrane now spans zero and is no more than ±1%. The change in TRT noted when using the RPE, however, still is considerably larger, with values as high as 8%.

Figure 6 shows an example of the RPE and Bruch's membrane segmentation on an on-axis and two off-axis scans. The segmented RPE and Bruch's membrane obtained for the two off-axis scans were transformed into the on-axis scan space by aligning the ILM. The RPE segmentation was seen to shift towards Bruch's membrane as the reflectivity of the PTOS reduced. Offsets in the pupil position along the vertical direction also resulted in reduction of the reflectivity of the PTOS, although the induced tilts were not immediately obvious in visual inspections of single B-scans. The appearance and automated segmentation of Bruch's membrane, however, remained unchanged. The left and right inclined scans in depicted in Figure 6 showed 6.35° and 7.11° angular deviations, respectively. The increase in the subfoveal TRT (region 9 in Fig. 2B) in the two scans when using the RPE and Bruch's membrane were 6.39 (2.46%) and 7.96 (3.04%) μm, and 3.19 (1.08%) and 4.00 (1.35%) μm, respectively.

Figure 7 provides a closer look at a section of the photoreceptors in an on-axis and two off-axis SDOCT images, where the variability in the brightness of the PTOS can be observed. Bruch's membrane (visualized as the bottom of the RPE/Bruch's membrane complex in SDOCT images) on the other hand, is not affected by the optical Stiles-Crawford effect.

Figure 8 shows a histogram of the incidence rates of angular deviations in the secondary set of 1545 SDOCT scans. Of the scans, 3% showed small tilts (0°–3°), 56% showed moderate tilts (4°–6°), and 41% of the scans showed larger tilts (≥6°).

Discussion

The off-axis acquisition of SDOCT images has been observed to result in an increase in TRT estimates[8] (Antony et al. *IOVS* 2014;55:ARVO E-Abstract 4791). While the axial measurement of TRT

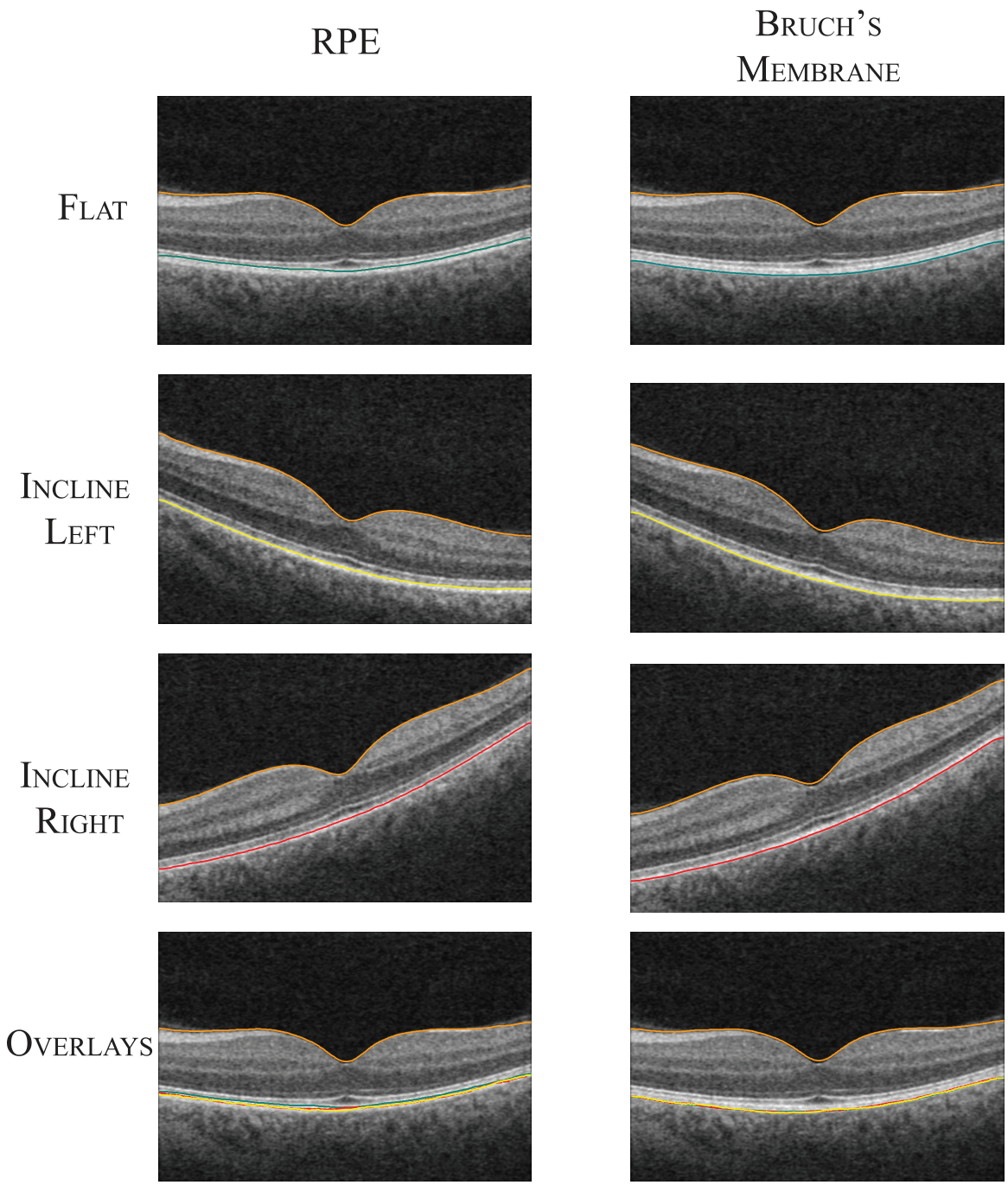

Figure 6. A central B-scan from an example on-axis and two off-axis scans obtained from a normal subject. The segmented RPE and Bruch's membrane have been overlaid on the B-scan. The surfaces were transformed into the on-axis scan space using the ILM. The *bottom row* shows the segmented surfaces overlaid on the on-axis scan.

in off-axis scans can induce an error due to the geometry of the structure, the thickness increase observed is larger than expected, indicating that this is not the only contributing cause for the anomaly. Addressing this artifact will ensure that the most precise OCT measurements are obtained. The careful acquisition of on-axis scans would eliminate the geometry-induced errors and improve the reproducibility of TRT estimates. However, this may not always be possible. For instance, media opacities may compel the use of an offset pupil position to obtain a scan with acceptable signal strength. Offsets in the

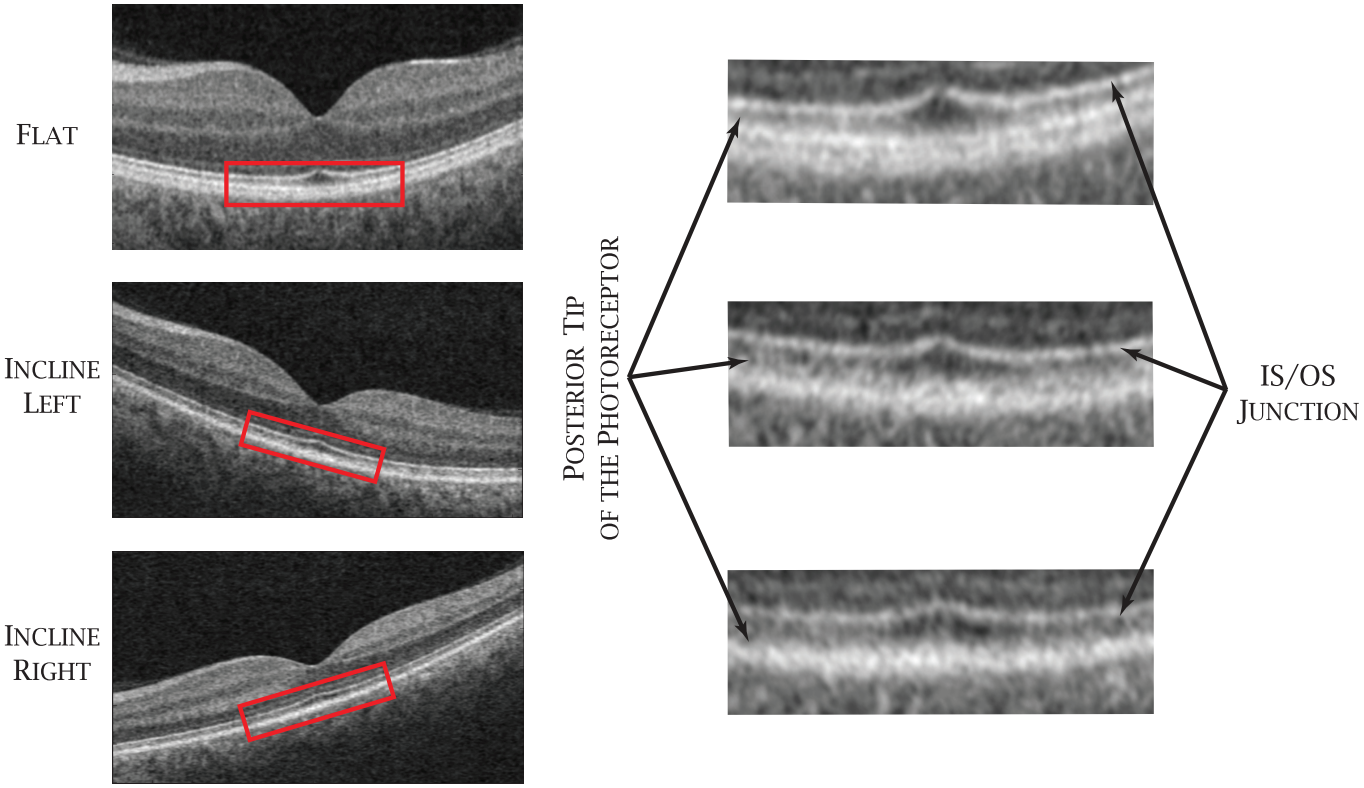

Figure 7. Central B-scans from an on-axis SDOCT volume and two off-axis SDOCT volumes with a closer look at the IS/OS and PTOS. The zoomed in images come from the sections marked in *red*.

pupil position along the vertical axis also are particularly difficult to detect, as the tilts will not be visible in the B-scans. However, the IS/OS junction and the PTOS will still exhibit diminished signals, which could impact the segmentation accuracy. Moreover, in highly myopic eyes, the signal strength is likely to vary even in on-axis scans due to the increased retinal curvature, with diminished signals

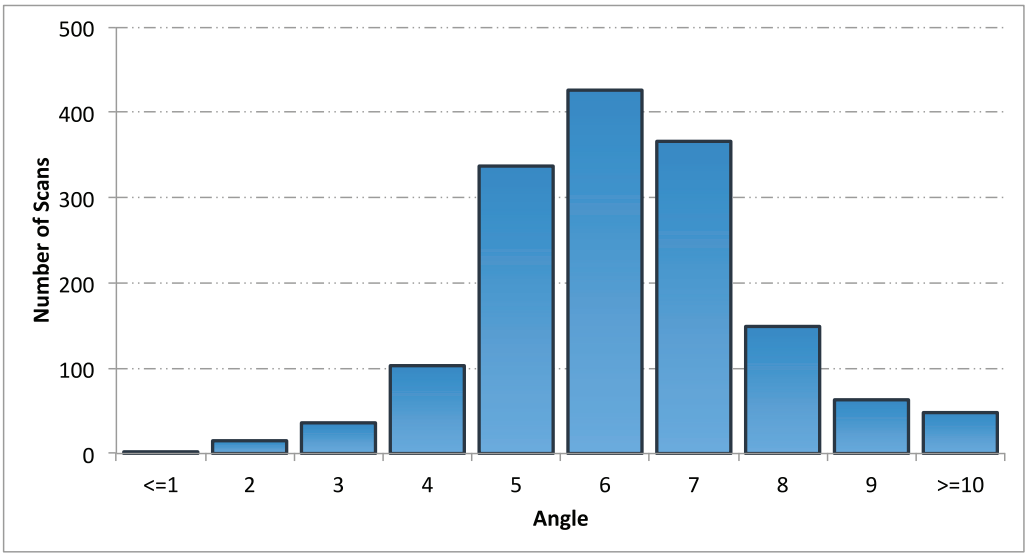

Figure 8. Summary of the incidence rates of angular deviation in 1545 scans (1545 patients) obtained from the Rotterdam study. A plane was fit to the sub-foveal region of the segmented RPE and the angular deviation of the plane with respect to the *z*-axis was computed.

being observed in the periphery of the B-scans. Similar situations also may arise in the presence of outer retinal pathologies.

The analysis of the secondary set of volumetric SDOCT images indicated that off-axis scans occurred frequently, where 41% of the scans showed angular deviations larger than 6°. Comparatively, the scans depicted in Figure 6 show an example of off-axis scans with 6° to 7° angular deviations, where the corresponding TRT obtained using the RPE showed increases of 2% to 3%. Furthermore, the scatterplot in Figure 7 indicates that the error in these scans could be as large as 6%.

Automated retinal segmentation approaches often use gradients at retinal layer boundaries (sharp transitions from dark to bright regions and vice versa) to segment the various surfaces.[19–22,26,27,35] Thus, surfaces that are marked by large image gradients are easier to detect. For instance, the transitions at the ILM and the IS/OS junction are quite distinct, making it easy to detect these surfaces and most automated segmentation approaches begin by segmenting these two surfaces. The gradient between the retinal nerve fiber layer and ganglion cell layer, on the other hand, is considerably smaller, making the identification of this surface quite difficult. Another commonly used feature is regional information, such as intensity.[19,27] For instance, the retinal nerve fiber layer is known to appear as a bright layer in SDOCT images, while the nuclear layers appear dark. The PTOS frequently is segmented instead of the RPE,[19–24] as 1) the gradient at the RPE is not as distinct as at the PTOS, and 2) the proximity between these two structures makes the incorporation of region-based features extremely challenging. Moreover, while it is possible to manually identify and differentiate the PTOS and the top of the RPE/Bruch's membrane complex in high-definition 2D B-scans, it is quite challenging to do the same in volumetric SDOCT scans due to the reduced signal-to-noise ratio. The change in reflectivity at this structure in off-axis scans affects the magnitude of the gradient, which in turn impacts the segmentation accuracy. Bruch's membrane on the other hand, is far more consistent in reflectivity and contrast; thus, many automated methods segment Bruch's while excluding the RPE altogether.[27,35–37] Furthermore, the development of automated segmentation approaches predated the accurate identification of these distinct structures, namely the PTOS and the RPE, in SDOCT images.[17,38] Thus, the results presented here highlight the need for automated methods to keep pace with new findings, especially when it pertains to the more accurate identification of structures in SDOCT images.

The general decrease in reflectivity of the PTOS due to the optical Stiles-Crawford effect is known, but variations in these directional properties across the retina are somewhat less understood. For instance, qualitative examinations of the images indicate that the PTOS at the fovea is more stable than peripheral regions of the image agrees with other reports in the literature.[39] However, we also note that the reflectivity in one half of the image frequently shows larger decreases than the other, something which, to our knowledge, has not been reported previously. This complex relationship and the considerable intersubject variability are evident in the scatterplot depicted in Figure 5.

The Cirrus HDOCT system defines the TRT using the RPE, while the Spectralis SDOCT system (Heidelberg Engineering, Heidelberg, Germany) uses Bruch's membrane. The TRT reproducibility in each of these systems has been studied individually,[40,41] and compared using the same subjects.[42] However, to our knowledge no studies have been conducted on scans acquired intentionally through peripheral pupil positions. This study is the first to characterize quantitatively the effect of off-axis SDOCT acquisition on subsequent automated analysis of retinal thickness estimates. The mean difference in TRT when using the RPE as the reference surface was significantly higher than when using Bruch's membrane, with similar trends evident in the CV and ICC analysis. It is important to note that the CV associated with the reproducibility of the TRT when using the RPE are under 2% and the ICC is consistently above 0.9 for the nine regions tested. However, the CV and ICC associated with the TRT derived using Bruch's membrane are consistently better. Moreover, the changes in TRT when using Bruch's membrane after accounting for the geometry-induced errors (depicted in Fig. 5B) are within ± 1%. Segmentation and registration inaccuracies are most likely responsible for this small residual error. The errors still noted when using the RPE as the reference surface are, however, much larger.

Although the reproducibility analysis may indicate that Bruch's membrane is the more stable reference surface, in practice, there are situations when the RPE could be the better choice. For instance, in the presence of pathology, such as pigment epithelial detachments (PED), the TRT obtained using Bruch's membrane would include the contents of the PED. This may not always be desirable, as it would impede the assessment of changes in the retinal tissue.

In conclusion, the TRT obtained using Bruch's

membrane is more robust than the measurements obtained using the RPE to off-axis perturbations. While the careful acquisition of on-axis SDOCT volumes would be preferable when assessing retinal structures, extenuating circumstances could make this impossible. In such situations, it is important to recognize the impact that the off-axis acquisition may impose on the visibility of retinal structures, such as the IS/OS and PTOS, as well as the challenges it subsequently may present to automated analysis methods.

Acknowledgments

The authors would like to thank Eric Strauss, MD, PhD for his assistance in completing this work.

Disclosure: **Bhavna J. Antony**, None; **Paul F. Stetson**, Carl Zeiss; **Michael D. Abramoff**, P; **Kyungmoo Lee**, None; **J.M. Colijn**, None; **Gabriële H.S. Buitendijk**, None; **Caroline C.W. Klaver**, None; **Austin Roorda**, P; **Brandon J. Lujan**, P

References

1. Huang D, Swanson EA, Lin CP, et al. Optical coherence tomography. *Science*. 1991;254:1178–1181.
2. Hee MR, Izatt JA, Swanson EA, et al. Optical coherence tomography of the human retina. *Arch Ophthalmol*. 1995;113:325.
3. Koizumi H, Spaide RF, Fisher YL, Freund KB, Klancnik JM, Yannuzzi LA. Three-dimensional evaluation of vitreomacular traction and epiretinal membrane using spectral-domain optical coherence tomography. *Am J Ophthalmol*. 2008;145:509–517.
4. Srinivasan VJ, Wojtkowski M, Witkin AJ, et al. High-definition and 3-dimensional imaging of macular pathologies with high-speed ultrahigh-resolution optical coherence tomography. *Ophthalmology*. 2006;113:5522–5528.
5. De Boer JF, Cense B, Park BH, Pierce MC, Tearney GJ, Bouma BE. Improved signal-to-noise ratio in spectral-domain compared with time-domain optical coherence tomography. *Opt Lett*. 2003;28:2067–2069.
6. Huang J, Liu X, Wu Z, Xiao H. Macular thickness measurements in normal eyes with time domain and fourier domain optical coherence tomography. *Retina*. 2009;29:980–987.
7. Wojtkowski M, Srinivasan V, Fujimoto JG, et al. Three-dimensional retinal imaging with high-speed ultrahigh-resolution optical coherence tomography. *Ophthalmology*. 2005;112:1734–1746.
8. Hariri A, Lee SY, Ruiz-Garcia H, Nittala MG, Heussen FM, Sadda SR. Effect of angle of incidence on macular thickness and volume measurements obtained by spectral-domain optical coherence tomography. *Invest Ophthalmol Vis Sci*. 2012;53:5287–5291.
9. Carl Zeiss Meditec, Inc. *Cirrus HD-OCT User Manual*, 4.0 ed. Dublin, CA: Carl Zeiss Meditec, Inc., 2009.
10. Keane PA, Mand PS, Liakopoulos S, Walsh AC, Sadda SR. Accuracy of retinal thickness measurements obtained with Cirrus optical coherence tomography. *Br J Ophthalmol*. 2009;93:1461–1467.
11. Sadda SR, Keane PA, Ouyang Y, Updike JF, Walsh AC. Impact of scanning density on measurements from spectral domain optical coherence tomography. *Invest Ophthalmol Vis Sci*. 2010;51:1071–1078.
12. Odell D, Dubis AM, Lever JF, Stepien KE, Carroll J. Assessing errors inherent in OCT-derived macular thickness maps. *J Ophthalmol*. 2011;2011:692574.
13. Stiles WS, Crawford BH. The luminous efficiency of rays entering the eye pupil at different points. *Proc R Soc B Biol Sci*. 1933;112:428–450.
14. Burns SA, Wu S, Delori F, Elsner AE. Direct measurement of human-cone-photoreceptor alignment. *J Opt Soc Am A*. 1995;12:2329–2338.
15. Van Blokland GJ. Directionality and alignment of the foveal receptors, assessed with light scattered from the human fundus in vivo. *Vision Res*. 1986;26:495–500.
16. Gao W, Cense B, Zhang Y, Jonnal RS, Miller DT. Measuring retinal contributions to the optical Stiles-Crawford effect with optical coherence tomography. *Opt Express*. 2008;16:6486–6501.
17. Staurenghi G, Sadda S, Chakravarthy U, Spaide RF. Proposed lexicon for anatomic landmarks in normal posterior segment spectral-domain optical coherence tomography. *Ophthalmology*. 2014:121:1572–1578.
18. Jonnal RS, Kocaoglu OP, Zawadzki RJ, Lee S-H, Werner JS, Miller DT. The cellular origins of the outer retinal bands in optical coherence tomography images. *Invest Ophthalmol Vis Sci*. 2014;55:7904–7918.
19. Garvin MK, Abràmoff MD, Wu X, Russell SR, Burns TL, Sonka M. Automated 3-D intraretinal

layer segmentation of macular spectral-domain optical coherence tomography images. *IEEE Trans Med Imag*. 2009;28:1436–1447.
20. Chiu SJ, Li XT, Nicholas P, Toth CA, Izatt JA, Farsiu S. Automatic segmentation of seven retinal layers in SDOCT images congruent with expert manual segmentation. *Opt Express*. 2010; 18:19413–19428.
21. Kajić V, Povazay B, Hermann B, et al. Robust segmentation of intraretinal layers in the normal human fovea using a novel statistical model based on texture and shape analysis. *Opt Express*. 2010; 18:14730–14744.
22. Bagci AM, Shahidi M, Ansari R, Blair M, Blair NP, Zelkha R. Thickness profiles of retinal layers by optical coherence tomography image segmentation. *Am J Ophthalmol*. 2008;146:679–687.
23. Fabritius T, Makita S, Miura M, Myllylä R, Yasuno Y. Automated segmentation of the macula by optical coherence tomography. *Opt Express*. 2009;17:15659–15669.
24. Lang A, Carass A, Hauser M, et al. Retinal layer segmentation of macular OCT images using boundary classification. *Biomed Opt Express*. 2013;4:1133–1152.
25. Lujan BJ, Roorda A, Knighton RW, Carroll J. Revealing Henle's fiber layer using spectral domain optical coherence tomography. *Invest Ophthalmol Vis Sci*. 2011;52:1486–1492.
26. Lee K, Niemeijer M, Garvin MK, Kwon YH, Sonka M, Abràmoff MD. Segmentation of the optic disc in 3D-OCT scans of the optic nerve head. *IEEE Trans Image Process*. 2009;29:159–168.
27. Antony BJ, Abràmoff MD, Lee K, et al. Automated 3D segmentation of intraretinal layers from optic nerve head optical coherence tomography images. In: *Proceedings of SPIE Medical Imaging 2010: Biomedical Applications in Molecular, Structural, Andgar Functional Imaging. Vol 7626*. 2010:76260U. doi:10.1117/12.843928.
28. Niemeijer M, Garvin MK, van Ginneken B, Sonka M, Abràmoff MD. Vessel segmentation in 3D spectral OCT scans of the retina. In: *Proceedings of SPIE Medical Imaging 2008: Image Processing. Vol 6914*. 2008:69141R.
29. Sonka M, Hlavac V, Boyle R. *Image Processing, Analysis and Machine Vision*, 3rd ed. Toronto: Thomson; 2008.
30. R Core Development Team. *R: A Language and Environment for Statistical Computing*. Vienna, Austria: R Foundation for Statistical Computing; 2013. Available at: http://web.mit.edu/r_v3.0.1/fullrefman.pdf.
31. Bhapkar VP. A note on the equivalence of two test criteria for hypotheses in categorical data. *J Am Stat Assoc*. 1966;61:228–235.
32. Wolfs RCW, Borger PH, Ramrattan RS, et al. Changing views on open-angle glaucoma: definitions and prevalences-the Rotterdam Study. *Invest Ophthalmol Vis Sci*. 2000;41:3309–3321.
33. Hofman A, Breteler MMB, van Duijn CM, et al. The Rotterdam Study: 2010 objectives and design update. *Eur J Epidemiol*. 2009;24:553–572.
34. Czudowska MA, Ramdas WD, Wolfs RCW. Incidence of glaucomatous visual field loss: a ten-year follow-up from the Rotterdam study. *Ophthalmology*. 2010;117:1705–1712.
35. Dufour PA, Ceklic L, Abdillahi H, et al. Graph-based multi-surface segmentation of OCT data using trained hard and soft constraints. *IEEE Trans Med Imag*. 2013;32:531–543.
36. Vermeer KA, van der Schoot J, Lemij HG, de Boer JF. Segmentation of retinal layers in volumetric OCT scans of normal and glaucomatous subjects. In: *Proceedings of SPIE, Ophthalmic Technologies XXI. Vol 7885*. 2011:78851B.
37. Zhang X, Yousefi S, An L, Wang RK. Automated segmentation of intramacular layers in Fourier domain optical coherence tomography structural images from normal subjects. *J Biomed Opt*. 2012; 17:046011.
38. Spaide RF, Curcio CA. Anatomoical correlates to the bands seen in the outer retina by optical coherence tomography. *Retina*. 2011;31:1609–1619.
39. Burns SA, Wu S, He JC, Elsner AE. Variations in photoreceptor directionally across the central retina. *J Opt Soc Am A*. 1997;14:2033–2040.
40. Garcia-Martin E, Pinilla I, Idoipe M, Fuertes I, Pueyo V. Intra and interoperator reproducibility of retinal nerve fibre and macular thickness measurements using Cirrus Fourier-domain OCT. *Acta Ophthalmol*. 2011;89:e23–e29.
41. Menke MN, Dabov S, Knecht P, Sturm V. Reproducibility of retinal thickness measurements in healthy subjects using spectralis optical coherence tomography. *Am J Ophthalmol*. 2009; 147:467–472.
42. Giani A, Cigada M, Choudhry N, et al. Reproducibility of retinal thickness measurements on normal and pathologic eyes by different optical coherence tomography instruments. *Am J Ophthalmol*. 2010;150:815–824.